Journal of Nanophotonics

SPIEDigitalLibrary.org/jnp

Efficiency of subwavelength imaging with multisegment nanolens

Pavel M. Voroshilov
Atiqur Rahman
Yuri S. Kivshar
Pavel A. Belov

Efficiency of subwavelength imaging with multisegment nanolens

Pavel M. Voroshilov,[a] Atiqur Rahman,[b] Yuri S. Kivshar,[a,c] and Pavel A. Belov[a,b]

[a] National Research University of Information Technologies, Mechanics and Optics, 197101, St. Petersburg, Kronverkskiy pr., 49, Russia

[b] Queen Mary University of London, School of Electronic Engineering and Computer Science, Mile End Road, London E1 4NS, United Kingdom

[c] The Australian National University, Nonlinear Physics Centre, Research School of Physics and Engineering, Canberra ACT 0200, Australia

pavel.belov@elec.qmul.ac.uk

Abstract. We analyzed capabilities and functionalities of a multisegment superlens recently suggested for long-distance transport of color images with subwavelength resolution. We studied the performance of three- and six-segment nanolens structures by analyzing numerically both transmission and reflection coefficients and by employing the full-wave simulations for a particular source arrangement. Our results suggest that such multisegment structures offer limited subwavelength imaging performance with a relatively narrow frequency band. [DOI: 10.1117/1.3611407]

Keywords: subwavelength imaging; metallic nanorods; stacked/multisegment nanolens; surface plasmon; near-field optics.

Paper 11026SSPR received Feb. 3, 2011; revised manuscript received Jun. 7, 2011; accepted for publication Jun. 22, 2011; published online Jul. 19, 2011.

1 Introduction

Subwavelength imaging is a subject of special interest in the study of negative-real refractive index material and photonic bandgap structures, and it attracted a lot of attention in recent times due to its potential applications in various areas. Such imaging results from the restoration of the evanescent field components that goes beyond the capability of a conventional dielectric lens which can handle only the far-field of a source and operates only with propagating waves. Therefore, the image formation is prohibited at the far-field region by a conventional lens. To overcome this problem, several solutions such as perfect lens,[1] silver superlens,[2] hyperlens,[3,4] and stimulated emission depletion fluorescence microscopes [5] have been put forward by various groups. Recently, imaging with a holey metallic plate [6] and a conducting sheet [7] have also been proposed. Another type of superlens that employs array of a silver nanorod was suggested for imaging in the visible range.[8] Such a lens operates through the excitation of surface plasmon polaritons (SPPs) on the individual rods. The improved multisegment superlens has been suggested for the color imaging capability,[9] and it can be employed to achieve magnification with a divergent arrangement of the nanorod assembly. Another salient feature of stacked superlens is that it can be employed to transport an image for a longer distance as compared to solid nanorods. The SPP excited in the first segment by a near-field source couples with the second segment, which then excites the next segment, and so on. This so-called domino effect in the plasmon excitation can eventually bring the source information to the other side of the device where a field-distribution similar to the source-field can be obtained. The above-mentioned devices pave

1934-2608/2011/$25.00 © 2011 SPIE

the way for the development of a new class of optical microscope capable of scanning the whole area of interest, and thus can save a considerable amount of time. This would eventually replace the incumbent ones which make the microscopy process very slow (10 μm/s) as it employs a single probe.

Subdiffraction imaging in the microwave and the infrared domains has been studied extensively, and theoretical and experimental results can be found in Refs. 10–12 where a subwavelength resolution is achieved by means of an array of metallic rods. Such an array helps only in guiding the evanescent waves from one interface to the other, whereas in Pendry's superlens amplification of the evanescent waves take place while the same is being guided through. The key point to achieve good imaging with a rodded medium is that the lens must operate in the canalization regime,[13] which can be ensured by having the rods abide by the Fabry–Pérot resonance condition, i.e, $L = n\lambda_g/2$, where λ_g is the guided wavelength and n is an integer number. Besides, the selection of source plays an important role while examining the fidelity of such a device. As discussed in Ref. 14, an injudicious choice of source might produce anomalous results[11] and mislead the readers. Electromagnetic waves in such an anisotropic medium do not experience cut-off and travel along the axis of anisotropy without suffering diffraction. It is quite remarkable that in a material of extreme anisotropy, a Fabry–Pérot resonance condition is satisfied simultaneously for all spatial harmonics, since the extraordinary waves in the medium travel along the rods with the same phase velocity, regardless of the transverse wave vector. The propagation mechanism in such a medium does not involve any resonance of the material parameters and hence resolution is mostly unaffected by material losses. While this is true in microwave range and under circumstance in IR range, the plasmonic effect and losses dominate in the visible range, and the resolution cannot be improved merely by reducing the spacing.[15]

In this paper we study the operational ability of a superlens, in the visible domain, formed by an array of silver nanorods arranged in stacks. First, we discuss the properties of the three-segment nanolens (Sec. 2). We define the regime where such a structure can be employed for the subwavelength imaging (Sec. 3) and also determine its bandwidth (Sec. 4). Next, we double the number of segments and study the six-segment structure (Sec. 5). We reveal that the six-segment nanolens can indeed be employed to guide an image at larger distances than the one- and three-segment structures, however, our results do not demonstrate the substantial bandwidth improvement.

2 Three-segment Stacked Nanolens

First, we consider a three-segment nanolens composed of three arrays of silver nanorods with the same parameters as in Ref. 9. The geometry of the nanolens structure is shown in Fig. 1(a). The lens was numerically modeled using a full-wave electromagnetic simulator CST^{TM} Microwave Studio. We have used the Drude model for relative permittivity of Ag defined as $\varepsilon_m(\omega) = \varepsilon_\infty - \omega_p^2/(\omega^2 + i\Gamma\omega)$ with $\varepsilon_\infty = 4.9638$, $\omega_p = 1.4497\times10^{16}$ rad/s and $\Gamma = 8.33689\times10^{13}$/s (Ref. 9) which gives us the relative permittivity value of $-9.121 + i0.304$ at the wavelength of 488 nm. The imaging capability of the lens was tested with the help of a cluster of in-phase point sources positioned on the rod-axis forming the letter "A," the same as in Ref. 9. Each point source is a small dipole polarized along the rod axis (X-axis) and placed 10 nm away from the array interface (front-interface). Although it was suggested in Ref. 9 that the device with a rod length of 50 nm, diameter 20 nm, and gap 10 nm operates at a frequency of 622 THz, we were unable to find any discernible image at this frequency. Figures. 2(a) and 2(b) show the field distributions at the source and the image planes of the nanolens. No discernible image in the form of the letter A is observed. This result does not support the expectation[9] for dramatic improvement of the imaging performance.

This inconsistency originates from the fact that our result was obtained by the full-wave simulation of finite-sized nanorod array presented in Fig. 1(a), whereas in earlier studies[9] the image was obtained under the assumption that linear arrays of nanorods composing the nanolens does not interact with each other. It is clear that in the considered case the interaction between

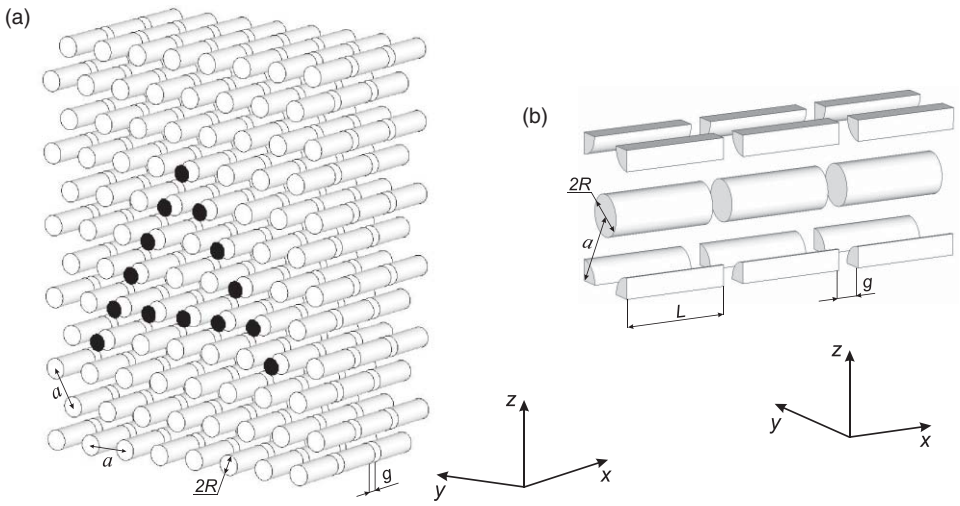

Fig. 1 (a) Geometry of three-segment stacked nanolens. The point sources arranged in the form of the letter *A* are placed on the respective rod axes and 10 nm away from the array interface. (b) A unit-cell employed to calculate the transmission and reflection coefficients.

the rows of nanorods is dramatic and this results in destruction of desired imaging capability. It is not possible to neglect interaction between different rows of nanorods.

In order to independently confirm the observed absence of imaging, we calculated dependencies of reflection and transmission coefficients on the transverse component of a wave vector of an incident *p*-polarized plane wave for an infinite (in *y*- and *z*−directions) three-segment

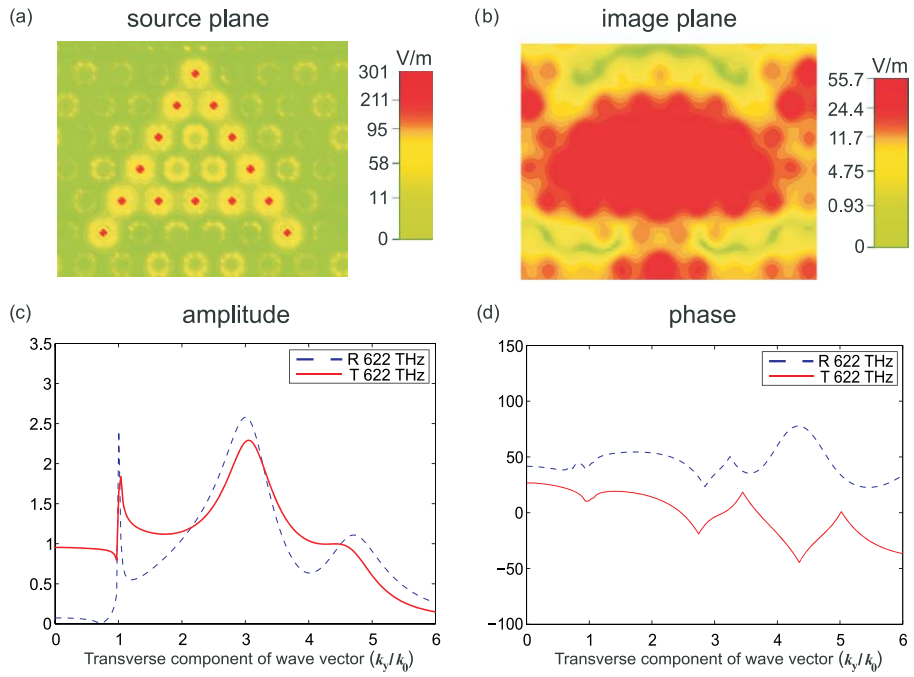

Fig. 2 Electric field distributions at the source (a) and the image (b) planes of the nanolens with a rod length of 50 nm and gap 10 nm. Amplitude (c) and phase (d) of reflection and transmission coefficients for an infinite array. The calculation was performed at 622 THz frequency as in Ref. 9.

array of nanorods. The unit-cell employed to calculate the coefficients is shown in Fig. 1(b) and the results are presented in Figs. 2(c) and 2(d). The transmission characteristic of a perfect imaging device has to be equal to 1 for a whole range of spatial harmonics. For real structures, the imaging is observed if the amplitude of transmission characteristic is close to unity and the phase does not vary dramatically over a certain range of spatial harmonics.[16] The amplitude of transmission coefficient in Fig. 2(c) has 3 local maximums and the phase in Fig. 2(d) significantly varies with slight changes of the transverse component of a wave vector. Such behavior by no means is compatible with satisfactory subwavelength imaging.

The problem with the stacked nanolens proposed in Ref. 9 is that the choice of the specific parameters does not allow to produce a convincing image and therefore this requires further study. A detailed step-by-step procedure of how to calculate the parameters of a single-segment nanolens for proper functioning in a particular band is given in Ref. 16 following an investigation that the lens exhibits problems in proper operation[8] for arbitrary coherent sources. The idea of this paper is to apply a similar procedure in order to determine the right parameters of the stacked lens that can improve the operation of the device. The earlier suggestion[9] to employ multiple segments in a bid to excite multiple resonances, and hence to have a very wide bandwidth, is not well justified since it assumes the absence of interaction between rows of nanorods. As will be shown below, the actual operation bandwidth of such a device is rather narrow.

3 Subwavelength Imaging Regime

As follows from Fig. 2, the original parameters of the stacked nanorod array are unable to produce the pattern of the transmission coefficient required for satisfactory subwavelength imaging.[16] Therefore, for proper imaging one needs to modify the parameters of the array (length of the rods and/or gap between them) and hence alter the pattern of the transmission and reflection coefficients. Another way could be to find another frequency band of operation different from that suggested in Ref. 9 with the existing parameters that would support the imaging operation of the device.

First of all, we opted for the latter in order to find the imaging capability of the device. We found that for a rod length of 50 nm and gap 10 nm, the device operates at 510 THz, in contrast to 622 THz as suggested in Ref. 9. The result of numerical simulation is presented in Fig. 3. The letter *A* is clearly seen in the image plane.

Secondly, we have observed that the decrease of the rod length leads to the increase of the operating frequency. The nanolens with 40 nm long nanorods operates at 555 THz (see Fig. 3).

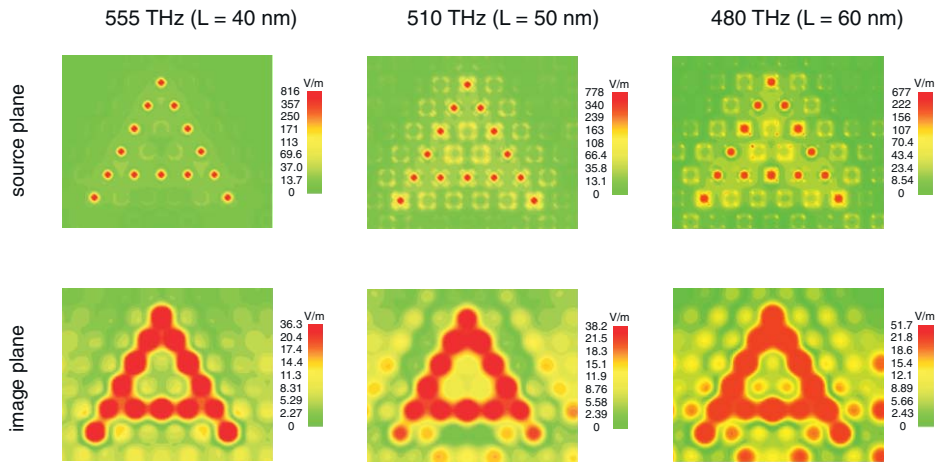

Fig. 3 Electric field distributions at the source and the image planes obtained for various lengths of the rod with a constant gap of 10 nm.

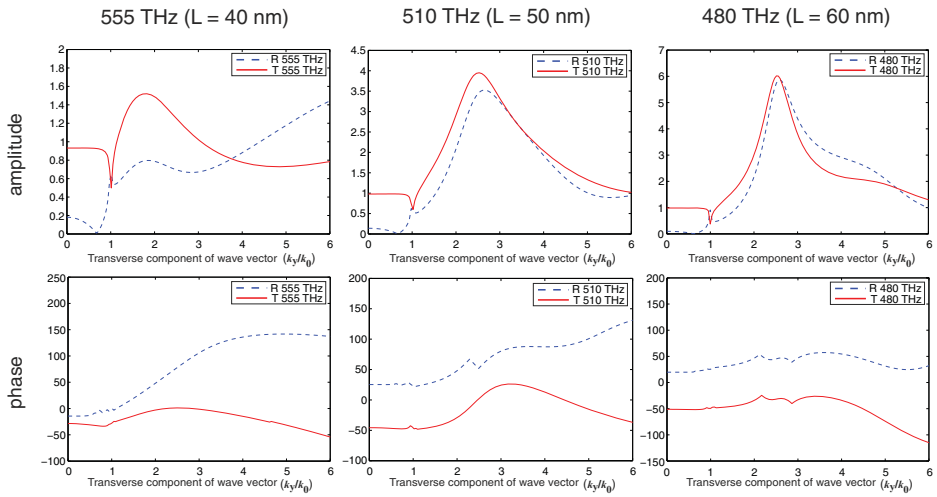

Fig. 4 Reflection and transmission coefficient pattern obtained for various lengths of the rod. The gap is kept equal to 10 nm.

The increase of the rod length leads to the decrease of the operating frequency: The nanolens with 60 nm long nanorods operates at 480 THz. However, as it can be seen from Fig. 3, the image appears slightly distorted by ripples due to excitation of surface waves. The further increase of the rod length leads to complete degradation of the image.

The observed phenomena can be clearly explained using the transmission coefficient dependencies on the transverse wave vector plotted in Fig. 4. These dependencies have single maxima for amplitude and slight variation of the phase. The increase of the rod length leads to an increase

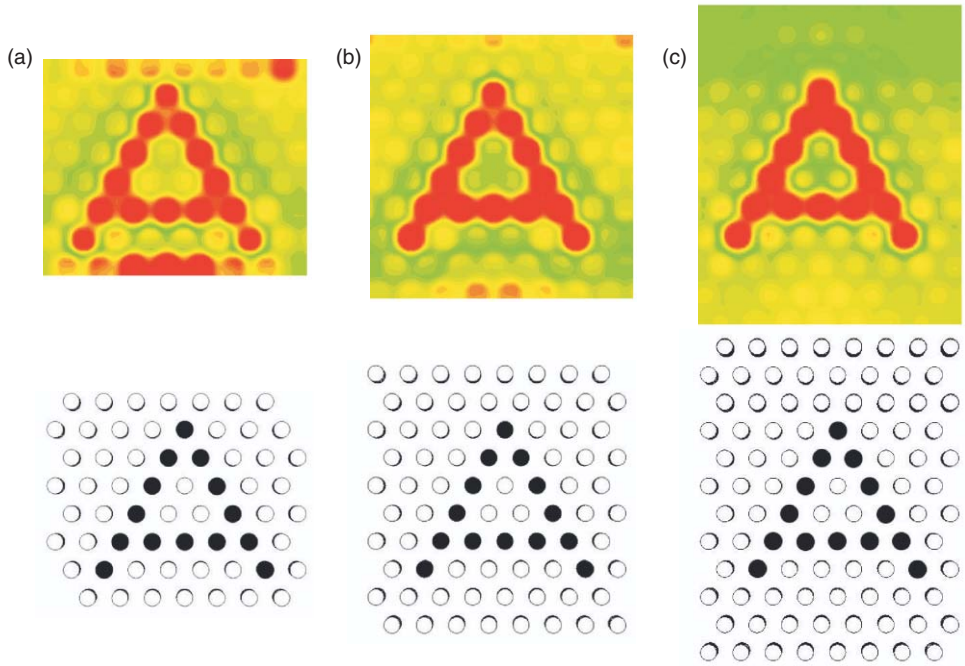

Fig. 5 Illustration of the influence of the aperture of a three-segment stacked nanolens with a rod length of 40 nm and gap 10 nm on image quality.

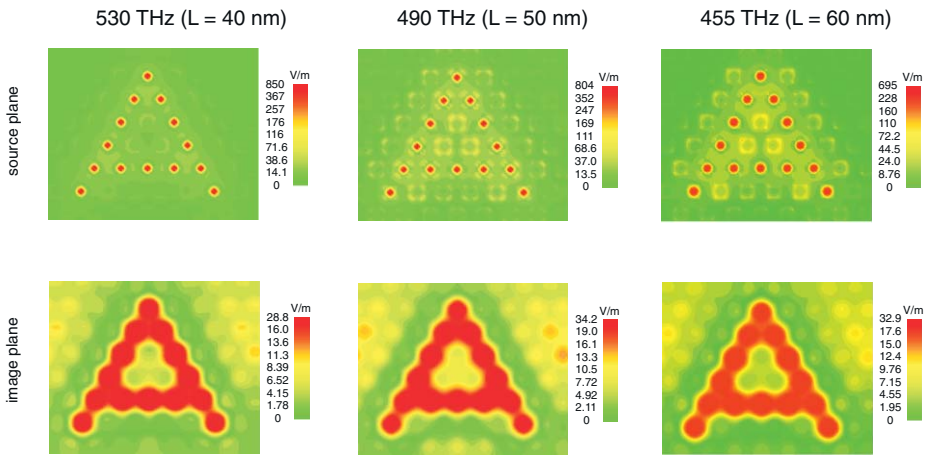

Fig. 6 Electric field distributions at the source and the image planes obtained for various lengths of the nanorod with intersegment gap of 5 nm.

of the maximum value of the transmission coefficient, and this results in the distortion of the image.

Here we have to emphasize that in our simulation, we experienced another source of image distortions. It was coming from diffraction on the finite-sized aperture of the lens. The influence of the nanolens aperture on imaging performance is illustrated in Fig. 5. Our observations have shown that the greater the aperture of the lens and the longer the distance between the source and the edges of the lens, the better the quality of the image. This conclusion is in good agreement with our previous studies of single-segment nanolenses.[17] That is why, in order to improve overall quality of images, in our simulations we have used geometry presented in Fig. 1(a) which corresponds to the best case [Fig. 5(c)] among three geometries shown in Fig. 5.

Interestingly, the decrease of the gap between the nanorods from 10 to 5 nm significantly improves the quality of imaging provided by the device, and leads to a decrease of operating frequency. The images obtained for the device with a 5 nm gap are shown in Fig. 6. The image quality and sharpness is better as compared to results presented in Fig. 3 for a nanolens with a

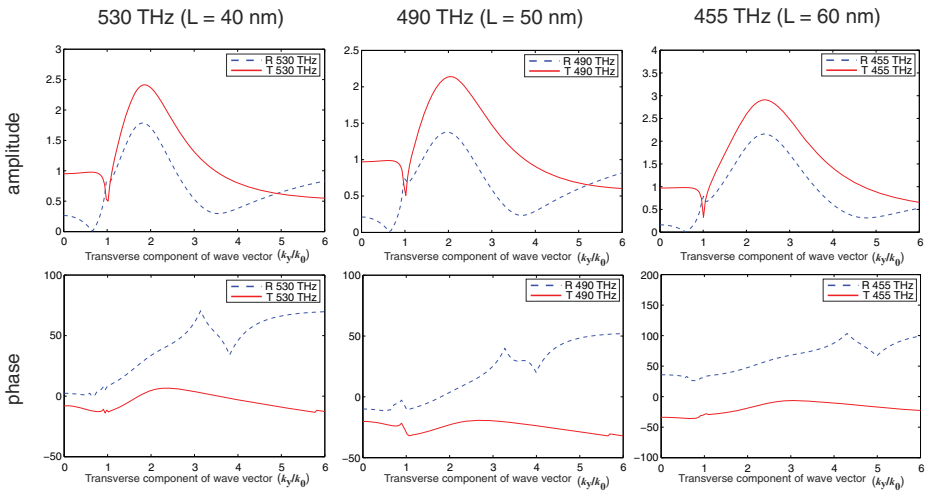

Fig. 7 Reflection and transmission coefficient pattern obtained for various lengths of the rod. Gap is kept equal to 5 nm.

Table 1 Operating range and bandwidth for various parameters of the stacked nanolenses.

Number of segments	Length (nm)	Gap (nm)	Frequency band (THz)	Bandwidth (%)
3	40	10	535 to 560	4.6
3	50	10	505 to 515	2.0
3	60	10	475 to 482	1.5
3	40	5	505 to 550	8.5
3	50	5	475 to 505	6.1
3	60	5	440 to 465	5.5
3	70	5	390 to 400	2.5
3	80	5	350 to 360	2.8
3	90	5	325 to 335	3.0
3	100	5	302 to 312	3.3
6	70	5	332 to 337	1.5
6	80	5	302 to 307	1.6
6	90	5	290 to 295	1.7
6	100	5	267 to 272	1.9

10 nm gap. The observed effect is clearly supported by the fact that the magnitude and phase patterns of transmission coefficient for a nanolens with a 5 nm gap shown in Fig. 7 have less variation than the ones in Fig. 4 for a 10 nm gap. The maximum value of the transfer function for 60 nm long rods drops from 6 to 3 with a decrease of gap from 10 to 5 nm. This results in significant improvement of the image quality for the nanolens formed by 60 nm long rods with a gap decrease (compare Figs. 3 and 6).

It should be noted that with the decreased gap between segments, the operating regime exhibits a redshift which can be attributed to the increased capacitance between the rods, resulting from the reduced gap.

4 Bandwidth Estimation

Field distributions in the image plane for various lengths of the nanorods and various gaps were calculated in the wide range of frequencies and analyzed. The analysis allowed us to summarize the main features of the nanolens operation in Table 1.

In particular, one can see that the increase of the nanorod length leads to a decrease of the operating bandwidth and a decrease of the central frequency of operation. The decrease of the gap between nanorods significantly improves the bandwidth of operation. In particular, for

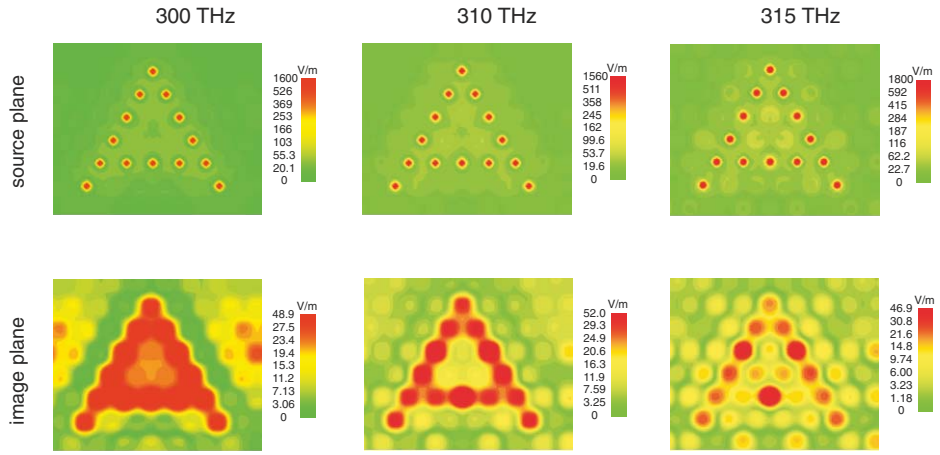

Fig. 8 Electric field distributions at the source and the image planes obtained at different frequencies for a rod length of 100 nm and a gap 5 nm.

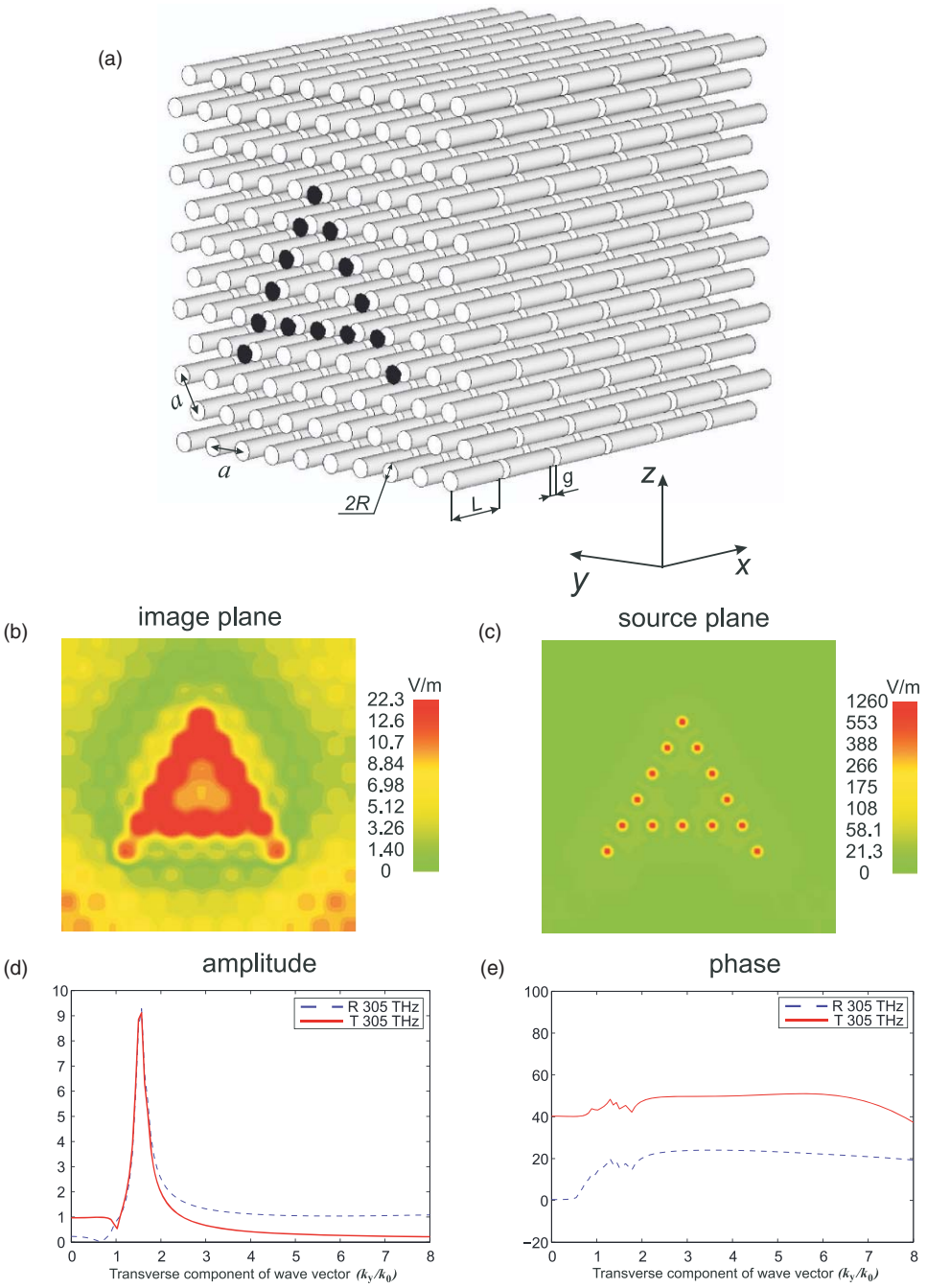

Fig. 9 (a) A geometry of a six-segment stacked nanolens. The point sources arranged in the form of the letter *A* are placed on the respective rod axis and 10 nm away from the array interface. Electric field distributions at the source (b) and the image (c) planes, and amplitude (d) and phase (e) of reflection and transmission coefficients as functions of a transverse wave vector obtained for a six-segment nanolens with an 80 nm long rod and a 5 nm gap at 305 THz.

60 nm long rods the bandwidth increases from 1.5% up to 5.5%. The decrease of the gap opens up the possibility to operate with longer nanorods and thus, transfer images to longer distances. For example, with a 10 nm gap no satisfactory images were observed if the length of the nanorod was greater than 60 nm and thus the maximum image transfer distance was (60 + 10 + 60 + 10 + 60) = 200 nm. However, with a 5 nm gap the images are observed even for

nanorods with a length about 100 nm and the transfer distance reaches (100 + 5 + 100 + 5 + 100) = 310 nm.

The typical imaging performance of the stacked nanolens with 100 nm long rods and 5 nm gap is illustrated in Fig. 8. This lens functions well over a bandwidth of 3% (303 to 312 THz). At frequencies lower than the band of operation the image of the letter *A* appears more bold as compared to regular images. This fact is illustrated in Fig. 8 by electric field distribution in the image plane at 300 THz. At the frequencies lower than the band of operation, the image appears distorted by ripples (see image plane electric field distribution at 315 THz in Fig. 8).

5 Six-segment Stacked Nanolens

Next, we double the number of segments in the nanorod assembly and examine the fidelity of the six-segment structure. Figure 9(a) shows a multisegment structure containing six segments with a rod-length of 80 nm in each segment and a gap of 5 nm between two consecutive segments. The image and source plane field distributions are also shown below. The distributions at the image plane fairly mimics that of the source plane. Here it should be noted that previously it was supposed that imaging is not possible with a device comprised of an even number of segments.[9] Besides, it was suggested that the bandwidth would improve with the increase in the number of segments, eventually leading to the color imaging capability of the device for a very large number of segments. Table 1 shows the calculated bandwidth for various parameters of the six-segment stacked nanolens. The bandwidth for a six-segment nanolens calculated for four different lengths of the nanorods is found to be around 1.5% to 1.9%, which is not among the highest values in the table and thus question the purported color imaging capability of the device. Thus, our results suggest that the existence of multiple resonance modes with multiple segments[9] may not be realized due to the interaction between different rows of the nanorods.

6 Conclusions

We have analyzed the imaging capabilities of the stacked nanolens formed by a lattice of nanorods. Such a multisegment nanolens was suggested earlier for transporting color images for long distances by virtue of the so-called domino plasmon effect. We have investigated three-and six-segment structures in order to reveal advantages and limitations of their operation. We have found that the six-segment nanolens can be employed to guide an image at larger distances than the three-segment structure, however, in contrast to the previous studies we did not confirm the bandwidth improvement. We have also calculated the transmission and reflection coefficients for infinite arrays of nanorods in order to have a deeper insight into the transmission characteristics of the lens. A resonance-free transmission coefficient magnitude and constant phase are mandatory to reproduce correctly the source field distributions. For a stacked nanolens, we have two parameters, the gap between consecutive segments and the length of the nanorod, which can be exploited in order to manipulate the transmission characteristics. We have shown that decreasing the gap significantly improves the imaging performance of the device: it increases the bandwidth and diminishes resonant excitation of surface waves. The adjustments of the nanorod length allows to tune the nanolens to operate at a particular frequency. Despite all the positive traits for the performance of such a stacked nanolens, the color imaging characteristic still remains elusive.

Acknowledgments

The authors acknowledge support from the Ministry of Education and Science of Russian Federation (Russia), EPSRC (UK), and Australian Research Council (Australia).

References

1. J. B. Pendry, "Negative refraction makes a perfect lens," *Phys. Rev. Lett.* **85**, 3966–3969 (2000).
2. N. Fang, H. Lee, C. Sun and X. Zhang, "Sub-diffraction-limited optical imaging with a silver superlens," *Science* **308**, 534–537 (2005).
3. I. I. Smolyaninov, Y.-J. Hung and C. C Davies, "Magnifying superlens in the visible frequency range," *Science* **315**, 1699–1701 (2007).
4. Z. Liu, H. Lee, Y. Xiong, C. Sun and X. Zhang, "Far-field optical hyperlens magnifying sub-diffraction-limited objects," *Science* **315**, 1686 (2007).
5. V. Westphal and S. W. Hell, "Nanoscale resolution in the focal plane of an optical microscope," *Phys. Rev. Lett.* **94**, 143903 (2005).
6. J. Jung, F. J. Garcia-Vidal, L. Martin-Moreno, and J. B. Pendry "Holey metal films make perfect endoscopes," *Phys. Rev. B* **79**, 153407 (2009).
7. C. Monzon, "Subwavelength imaging with conducting sheets," *Phys. Rev. Lett.* **102**, 173901 (2009).
8. A. Ono, J. Kato, and S. Kawata, "Subwavelength optical imaging through a metallic nanorod array," *Phys. Rev. Lett.* **95**, 267407 (2005).
9. S. Kawata, A. Ono, and P. Verma, "Subwavelength colour imaging with a metallic nanolens," *Nature Photon.* **2**, 438–442 (2008).
10. P. A. Belov, Y. Zhao, S. Tse, P. Ikonen, M. G. Silveirinha, C. R. Simovski, S. Tretyakov, Y. Hao, and C. G. Parini, "Transmission of images with subwavelength resolution to distances of several wavelengths in the microwave range," *Phys. Rev. B* **77**, 193108 (2008).
11. G. Shvets, S. Trendafilov, J. B. Pendry, and A. Sarychev, "Guiding, focusing, and sensing on the subwavelength scale using metallic wire arrays," *Phys. Rev. Lett.* **99**, 053903 (2007).
12. M. Silveirinha, P. A. Belov, and C. R. Simovski, "Subwavelength imaging at infrared frequencies using an array of metallic nanorods," *Phys. Rev. B* **75**, 035108 (2007).
13. P. A. Belov, C. R. Simovski, and P. Ikonen "Canalization of subwavelength images by electromagnetic crystals," *Phys. Rev. B* **71**, 193105 (2005).
14. A. Rahman, P. A. Belov, M. G. Silveirinha, C. R. Simovski, Y. Hao, and C. G. Parini, "Role of Fabry-Perot resonance and shielding in subwavelength imaging performance of multiwire endoscopes," *Appl. Phys. Lett.* **94**, 031104 (2009).
15. M. Silveirinha, P. A. Belov, and C. R. Simovski, "Ultimate limit of resolution of subwavelength imaging devices formed by metallic rods," *Optics Letters* **33**, 1726–1728 (2008).
16. A. Rahman, P. A. Belov, and Y. Hao, "Tailoring silver nanorod arrays for subwavelength imaging of arbitrary coherent sources," *Phys. Rev. B* **82**, 113408 (2010).
17. A. Rahman, S. Yu. Kosulnikov, P. A. Belov, Y. Hao, and C. Parini, "Subwavelength optical imaging with an array of silver nanorods," *J. Nanophoton.* **5**, 051601 (2011).

Biographies and photographs of the authors not available.